Materials Research Proceedings 41 (2024) 1027-1037 https://doi.org/10.21741/9781644903131-113

Development of the cross-section moment in air-bending

POKKA Aki-Petteri[1,a *], KESTI Vili[2,b], TROIVE Lars[2,c] and KAIJALAINEN Antti[1,d]

[1]University of Oulu, Materials and Mechanical Engineering, P.O. Box 4200, 90014 Oulu, Finland

[2]SSAB Europe, Rautaruukintie 115, 92101 Raahe, Finland

[a]aki-petteri.pokka@oulu.fi, [b]vili.kesti@ssab.com, [c]lars.troive@ssab.com, [d]antti.kaijalainen@oulu.fi

Keywords: Air Bending, Steel, DIC, Strain Distribution, Bending Moment

Abstract. The engineering potential of air-bending as a sheet-metal forming process has been limited by certain challenges related to high-strength steels, strain localization, surface defects, "multi-breakage" and bend shape. The phenomena related to these challenges are not yet fully understood, as the conventional test methods have not provided sufficient data for in-depth analysis of the material behavior in air-bending. In this study, nine thermomechanically rolled steel grades are bent in an air-bending test setup using three different punch radii, and Digital Image Correlation for strain measurement on the outer surface. The development of the cross-section moment is measured from the force-displacement curve. A connection is found between the developments of the cross-section moment, strain distribution and multi-breakage, as well as the strain-hardening properties of the material. The presented results illustrate the potential for predicting bending behavior based on the force-displacement curve, that could be achieved with better understanding of the physics related to the air-bending process.

Introduction

Air-bending is a widely used forming method for sheet metals because it is fast, cost-effective, and flexible. A wide range of bending angles can be obtained without tool modifications just by controlling punch displacement. The radius of the bend is usually controlled by altering the punch radius. However, the final shape of the bend also depends on the material properties. The distribution of strain and curvature on the outer bend surface can vary greatly depending on the strain-hardening properties of the material. Materials with a low strain-hardening tend to produce more localized strain distributions, leading to increased peak strain [1] and punch-sheet separation at the centerline ("multi-breakage") due to decreased inner radius [2].

The multi-breakage and punch-sheet separation have been known as a phenomenon for a long time and studied by several authors [3-10]. However, research on the root of the phenomenon, i.e., the development of the strain and moment distributions, has been relatively scarce. Strain distributions in air-bending have been studied by several authors [1,2,10-17], as is the case for the development of the bending moment in air-bending [4,18,19]. However, to the knowledge of the authors, development of the strain and bending moment have not been studied simultaneously before. Therefore, research in this area is necessary.

In this study, 6 mm thick steel sheets (with yield strength between 355 – 1700 MPa) are bent in a 3-point bending test setup in a Zwick universal tensile test machine. Three different punch radii are used. Digital Image Correlation (DIC) is used for measuring the strain on the outer bend surface. The aim of the paper is to investigate the connection between the cross-section moment, strain distribution development and multi-breakage. The effects of tool geometry and material properties on the development of the cross-section moment are also investigated.

Materials Research Proceedings 41 (2024) 1027-1037 https://doi.org/10.21741/9781644903131-113

Experimental procedure

Nine thermomechanically hot-rolled steel grades are tested in this study. Tensile and mechanical properties are provided in Table 1. Both longitudinal and transverse orientations are included in this study, referring to the orientation of the material's rolling direction within the test setup. In this study, the longitudinal (0°) tensile test is defined by the principal strain being parallel to the rolling direction, while the longitudinal (RD) bend test refers to the bend axis being parallel with the rolling direction. Consequently, the direction of the major strain on the outer bend surface is aligned with the rolling direction in the transverse bend orientation, meaning that transverse (TD) bends are compared to longitudinal (0°) tensile properties, and longitudinal (RD) bends to the transverse (90°) tensile properties. A schematic representation of the orientations is presented in Fig. 1.

Table 1. Sheet thicknesses (t) and mechanical properties of the tested materials. The yield strength (R_e), ultimate tensile strength (R_m), uniform elongation (A_{gt}), total elongation with 40 mm gage length (A_{40}), and strain hardening exponent ($n_{1\text{-}Ag}$) were measured from tensile tests in a previous publication by the authors [1]. The minimum bend radii to 90° bend angle (R_{min}) were provided by a steel manufacturer for corresponding grades.

Material	t [mm]	R_e [MPa]	R_m [MPa]	A_{gt} [%]	A_{40} [%]	$n_{1\text{-}Ag}$ [-]	R_{min}
St355 (0°/90°)	5.94	438/480	496/502	16.7/15.7	32.7/31.2	0.162/0.150	0.3 t
St500 (0°/90°)	5.92	585/628	653/669	12.1/10.8	26.9/25.4	0.120/0.106	0.8 t
St700 (0°/90°)	6.04	785/818	864/907	6.40/4.95	18.2/15.2	0.064/0.057	1 t
St900_1 (0°/90°)	5.99	974/1024	1042/1142	3.67/2.73	13.4/8.2	0.038/0.041	3 t
St900_2 (0°/90°)	5.93	1034/1067	1130/1151	4.38/3.52	13.9/11.4	0.036/0.032	3.5 t
St1100_1 (0°/90°)	6.01	1132/1127	1161/1172	5.20/5.20	15.4/13.8	0.044/0.045	3.5 t
St1100_2 (0°/90°)	5.93	1098/1111	1253/1271	3.62/3.11	12.1/10.8	0.046/0.042	3 t / 4 t
St1500 (0°/90°)	5.68	1537/1500	1761/1780	4.37/4.00	10.6/9.4	0.051/0.054	6 t
St1700 (0°/90°)	6.09	1740/1680	1958/1975	3.77/3.65	9.6/9.0	0.041/0.052	6 t

The bend specimens were cut from the 6 mm thick sheets into 80 mm wide rectangular strips using a water jet cutter. The specimen width of 80 mm is enough to ensure plane strain condition at the center of the bend. The specimens were bent at room temperature using a Zwick 100 kN universal tensile test machine equipped with a purpose-built bending tool setup, shown in Fig. 2a. The setup allows measurement of the bending force and punch stroke, as well as allowing a continuous unobstructed line-of-sight between the DIC cameras and the measured specimen surface, allowing measurement of strain and displacement throughout the test, as illustrated in Fig. 2b. A schematic representation of the bending geometry is presented in Fig. 3, and the parameters of the three tool setups are presented in Table 2. The shoulders of the die are lubricated using a PTFE spray, and they rotate freely in their sockets. In each setup, the specimens were bent until they either fractured or reached the bend angle of α_{end}. Two repeat tests were conducted for each combination of tool setup, material, and bend orientation.

The bend angle was calculated according to ISO 7438 [20], taking into account the vertical elasticity of the setup (rigidity of both the tensile test machine and the bending tools), measured at 51.9 kN/mm. The cross-section moment M is determined from the bending force (vertical load) F, bend angle α, die-width W_d, punch radius R_p and die shoulder radius R_d according to Eq. 1 [18].

$$M = \frac{F \cdot [W_d/2 - (R_p + R_d)\ \sin(\alpha/2)]}{2\cos^2(\alpha/2)}. \quad (1)$$

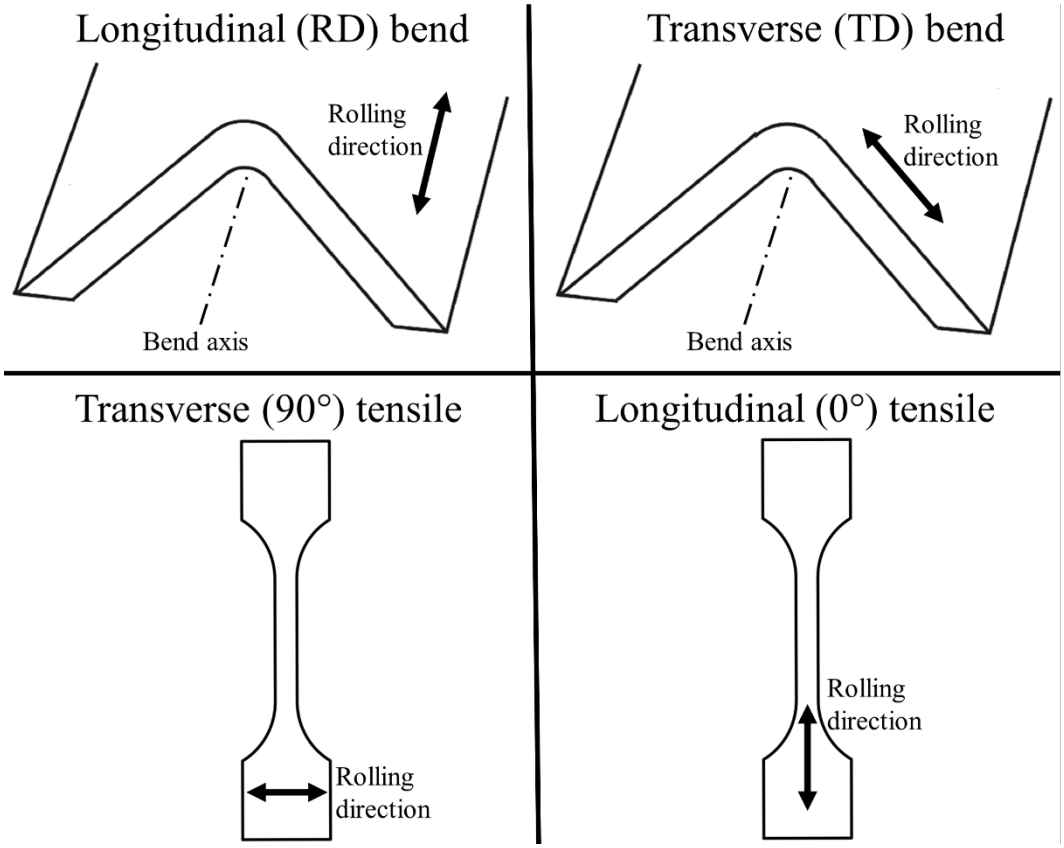

Fig. 1. The longitudinal and transverse orientations in tensile and bending tests.

The specimens were painted with a black-and-white speckle pattern to improve the DIC measurement accuracy and reliability. The DIC system used in this study was LaVision Strainmaster, with DaVis 8.4 software, and two monochrome CCD cameras of 2456 × 2058 pixel resolution. The DIC recording and processing parameters are presented in Table 3. Fig. 2c provides an example of a strain map of the bent surface measured by DIC. For each captured DIC image, the principal strain values were extracted from three sections across the bend, as illustrated in Fig. 2c. The peak bending strain ε_{b_max} at each point in time was calculated as the average of the peak values of the three sections. More information of the test setup and the determination of the peak strain can be found in earlier work by the authors [1,2,17].

In order to track the punch-sheet separation associated with the multi-breakage, the displacement of the sheet in the out-of-plane direction (Z-displacement) is measured by DIC. The values are extracted from a 1×1 mm^2 area on the outer bend surface at the centerline, as illustrated in Fig. 2c. As the punch is stationary in the setup (after adjusting for the vertical elasticity), the measured Z-displacement is a result of a combination of thinning and punch-sheet separation. The derivatives of the peak strain, cross-section moment and Z-displacement were calculated using the central difference method, smoothed by taking the moving average of 9 datapoints.

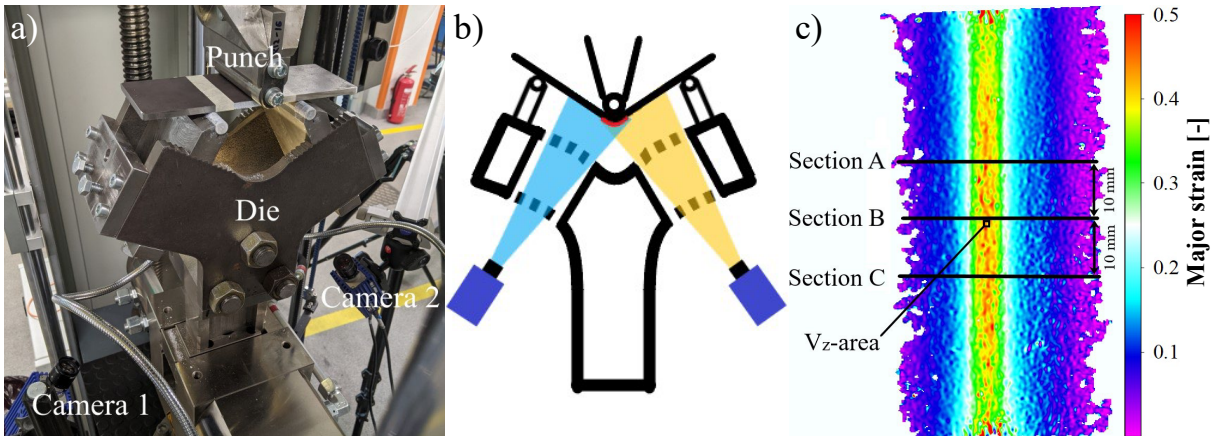

Fig. 2. a) The bending test setup, b) positioning of the DIC cameras, and c) areas for extracting the strain (sections A – C) and Z-displacement (V_z) on a DIC-measured strain map of the St1100_1 (RD) at 90° bend angle, using a punch radius R_p = 2 t.

Table 2. Bending tool setup parameters: Punch radius (R_p), die width (W_d), radius of the die shoulders (R_d), vertical speed of the punch (V_p) and the final bend angle before unloading (α_{end}).

Tool setup	R_p	W_d [mm]	R_d [mm]	V_p [mm/s]	α_{end} [°]
1	4 mm ≈ 0.66 t	90	6	1	120
2	12 mm ≈ 2 t	90	6	1	100
3	24 mm ≈ 4 t	110	6	1	110

Table 3. Recording and processing parameters for the DIC system.

DIC system and software	LaVision Strainmaster (Stereo DIC), DaVis 8.4
Sensor, digitization, imaging rate	2456 × 2058, 12-bit, 2 Hz
Lens, imaging distance, image scale	35 mm C-mount, 0.37 – 0.57 m, 21 – 30 pixels/mm
Subset size, step size, VSG	15x15 pixels, 5 pixels, 35 pixels
Strain window, smoothing method	5x5 data points, 2nd order polynomial fit
St.dev of principle strain	450 - 1700 microstrain
Interpolation, shape function, algorithms	6th order spline interpolation; affine shape function; LSM (iterative least squares matching) algorithm based on optical flow estimation

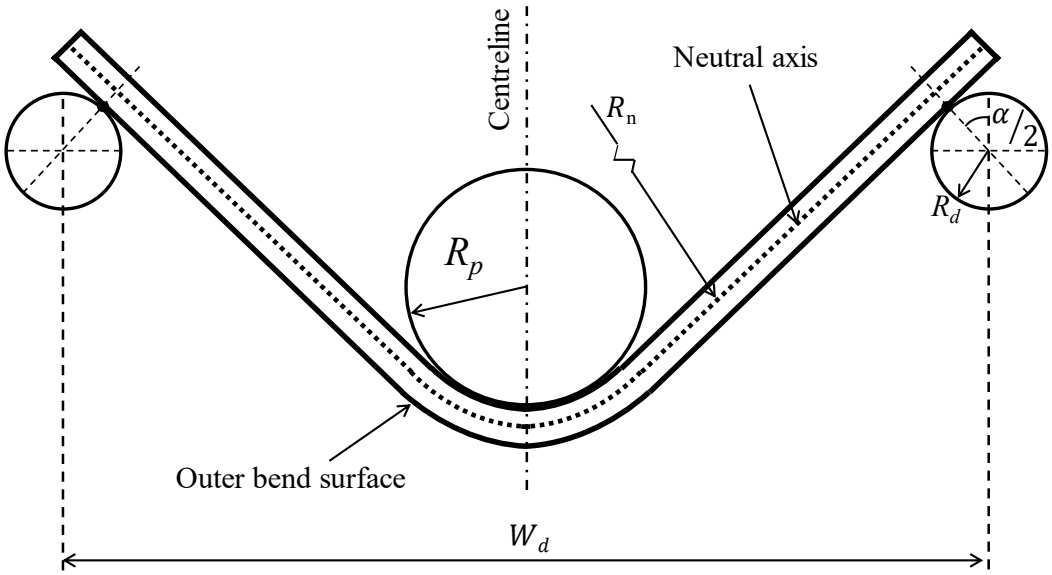

Fig. 3. The geometry and parameters of the bending tools and the workpiece.

Results and discussion

As seen in Fig. 4, the strain distributions for St700 are similar at 30° bend angle, regardless of the punch radius. However, as the bend angle increases, the impact of the punch radius on the strain distribution becomes apparent. For punch radius R_p = 0.66 t, the deformation is mainly concentrated at the center, creating a narrow strain distribution with a large peak. In contrast, using a larger punch produces a wider strain distribution with a lower peak. In fact, when using the largest punch (R_p = 4 t), the peak strain does not increase at all between the bend angles of 60° and 90°, since the deformation is only increasing from the sides.

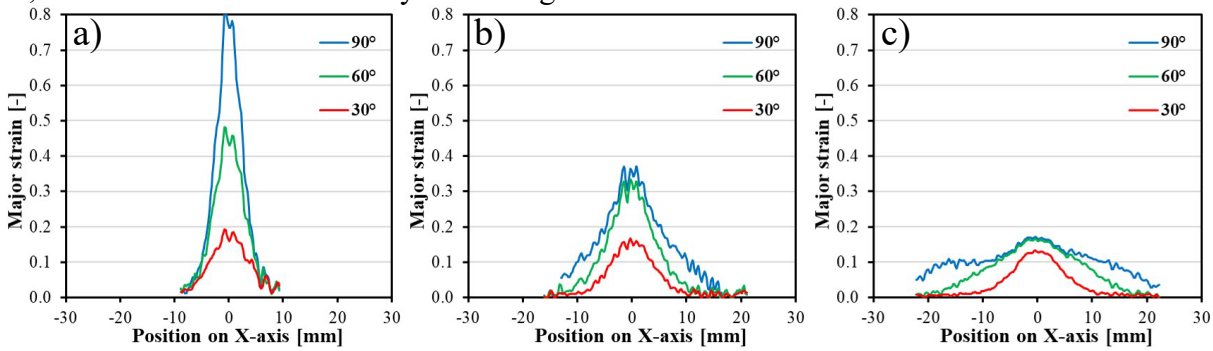

Fig. 4. Strain distributions from section B of St700 (RD) at 30°, 60° and 90° bend angle, bent using a) R_p = 0.66 t, b) R_p = 2 t and c) R_p = 4 t.

Fig. 5 presents the development of the peak strain ε_{b_max}, cross-section moment M, Z-displacement V_z and their first derivatives for the St355, St700 and St900_1 grades bent using punch radius R_p = 2 t. From Fig. 5a and Fig. 5d it can be seen that the strain rate ($d\varepsilon_{b\_max}/d\alpha$) for the St355 grade starts out higher compared to the St700 and St900_1 grades, but starts to gradually decrease after 10° bend angle, before reaching a steady state ($d\varepsilon_{b\_max}/d\alpha = 0$) at 90° bend angle.

The development of the peak strain and strain rate for the St700 and St900_1 grades starts out roughly identical but diverge after 10° bend angle. For both St700 and St900_1, the peak of the strain rate is reached between 30 – 40° bend angle, after which the strain rate starts to decrease. For St700, the strain rate decreases gradually until the steady state is reached at around 80° bend angle. For the St900_1 grade, the strain rate first decreases after around 40° bend angle, then stays roughly constant between 50° – 80° before starting to decrease again.

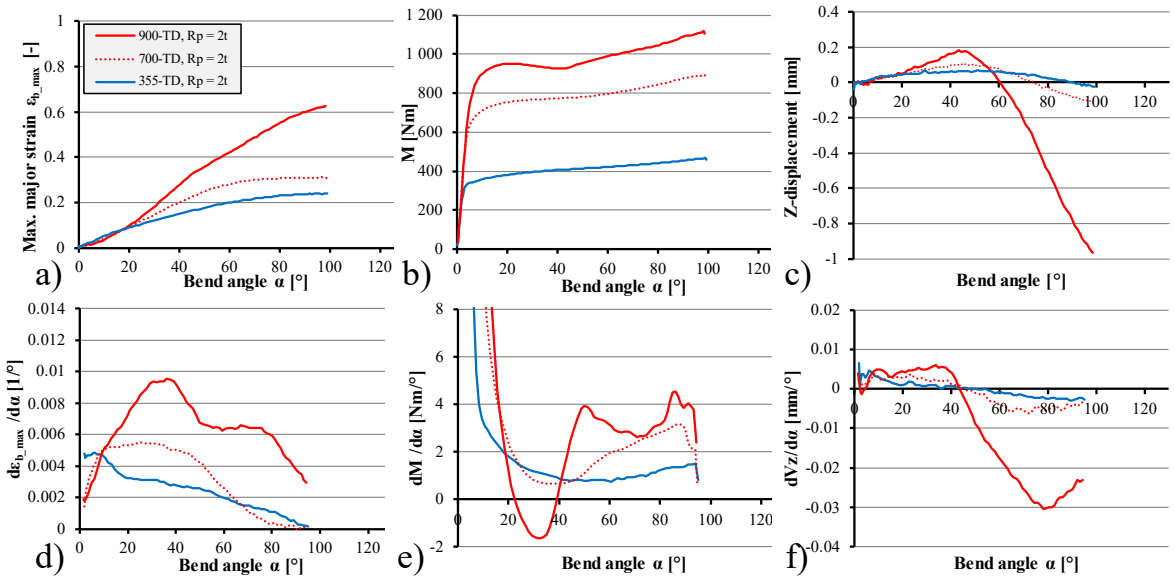

Fig. 5. Development of a) the peak strain, b) cross-section moment, c) Z-displacement, d) peak strain derivative, e) moment derivative and f) Z-displacement derivative, measured from St355, St700 and St900_1 bent in the transverse (TD) orientation, using punch radius R_p = 2 t.

Looking at Fig. 5b and Fig. 5e, it is seen that both St700 and St900_1 reach a minimum in the moment derivative dM/dα at around 30 – 40° bend angle, after which the moment derivative starts to increase. For St900_1, the rapid increase of the moment derivative is followed by a steady decrease between 50° – 80°, before starting to increase again towards the end of the test. For the St700 grade, the moment derivative increases gradually between 40° – 90°. For the St355 grade, the changes in the moment are more gradual, and the minimum of the moment derivative is reached around 60°.

Fig. 5c and Fig. 5f show the development of the Z-displacement and its derivative. For the St900_1 grade, the displacement increases at a roughly constant rate until around 40° bend angle, meaning that the outside surface moves towards the punch due to thinning. After 40°, the Z-displacement starts to decrease, meaning that the outside surface of the sheet moves away from the punch, i.e., there is a loss of contact between the punch and the sheet at the centerline (x = 0 mm). After around 80° bend angle, the derivative of the Z-displacement starts to increase again. Similar observations can be made for the St700 and St355 grades, albeit on a smaller scale.

By comparing the derivative curves in Fig. 5, an observation can be made that the moment derivative dM/dα minimums (at around 30°, 40° and 60° for St900_1, St700 and St355, respectively) roughly coincide with the points at which the derivatives of the peak strain and the Z-displacement start to decrease. These can all be attributed to the wrap-around, and the consequent change in the loading scheme. At the start of the bending process, the deformation is mostly localized at the centerline. As the peak strain increases, the inside radius of the sheet decreases. After a certain level of peak strain is reached, the inside radius of the sheet becomes equal to the punch radius and the sheet "wraps around" the punch, meaning that the loading scheme changes from 3-point bending to something closer to 4-point bending. As the contact points shift further apart, the moment distribution changes, and the bending moment is distributed to a larger area. The contact point shift is also related to the so-called "multi-breakage" effect, where the inside radius of the sheet becomes smaller than the punch radius, leading to a loss of the punch-sheet contact at the centerline, as well as a quick shift in the loading scheme and moment distribution [4]. Due to the implications of the wrap-around on the moment distribution, it is assumed that the wrap-around angle coincides with the derivative dM/dα minimums.

The increase in the dM/dα after the wrap-around can be explained from two perspectives – the internal and external bending moments. The internal bending moment of the material must be the same as the external moment applied by the tools. Due to strain hardening and the shifting of the neutral axis towards the inside surface, the internal bending moment must increase throughout the bending process to continue deforming the material. Consequently, the external moment applied to the material must also increase. However, due to the contact point shift in the wrap-around, which "forces" a wider moment distribution with a "dull" peak (as in 4-point bending), achieving the increased moment requires more force compared to the 3-point bending prior to wrap-around. This is seen as the increase in the calculated moment derivative dM/dα.

The change of the moment distribution in the wrap-around also promotes distribution of strain into a larger area, which inhibits strain localization at the centerline, indicated by the decrease of the strain rate $d\varepsilon_{b\_max}/d\alpha$ after the wrap-around angle (dM/dα minimum) for all the tested grades. The decrease in the Z-displacement after wrap-around, as seen most clearly for the St900_1 grade, is an indication of punch-sheet separation at the centerline, which is characteristic to a pronounced multi-breakage effect. The increase in the derivative of the Z-displacement of the St900_1 grade after 80° can be explained by looking at the derivatives of the strain and moment. The decrease in the strain rate and increase of the moment derivative indicate that there is again a change in the moment distribution due to the contact points moving further away from the centerline. This "second wrap-around" means that the sheet at the centerline starts to approach a steady state as the derivatives of the peak strain and Z-displacement start to approach zero. The unique development of the contact point positions may also be the reason behind the polygonal "nut-like" shape of the bent sheet that has been observed for the St900_1 and other ultra-high strength steel grades in previous studies [2,5,7,8].

The differences between the materials in the development of the strain, moment and Z-displacement can be attributed to differences in the strain-hardening properties. Materials with greater strain-hardening have greater resistance to strain localization. This leads to wider strain distributions with lower peak strain. As the peak strain is lower, the inside radius also decreases at a slower rate. Consequently, the wrap-around happens later. This is observed in the derivative curves in Fig. 5. For St900_1, the grade with the lowest strain-hardening, the effects related to the wrap-around start around 30 – 40°, for the St700 at around 40 – 50°, and for the St355 grade (greatest strain-hardening) around 50 – 60°.

The dM/dα minimum values seem to be linked to the strain rate ($d\varepsilon_{b\_max}/d\alpha$) maximum values at the wrap-around angle (30 – 40°), as well as the strain-hardening properties of the material. St900_1 (lowest strain-hardening) produces the most localized strain distribution with the highest peak strain and strain rate maximum, while also showing the lowest minimum dM/dα value. On the other hand, St355, the grade with the highest strain-hardening, produces the lower peak strain and strain rate, while also showing the highest minimum dM/dα value at the wrap-around angle. The negative dM/dα before wrap-around (as seen for the St900_1 grade) may be compared to strain softening, in that it is clearly connected to accelerated strain localization at the centerline, which is not a desirable property in terms of bendability. This "softening" effect could be due to development of shear-bands below the surface. However, even though defects (shear bands and notches) could be seen on the surface of the St900_1 (TD) specimen after the test, the investigations performed for this paper cannot confirm that the shear bands initiated before the wrap-around angle. To confirm this conjecture, the tests should be interrupted before the wrap-around angle to inspect the cross-sections of the specimens.

A localized strain distribution has been connected with the more pronounced multi-breakage effect [2]. The strain distribution development has also been previously found to correlate with the global formability properties of the material (e.g., strain-hardening exponent) [1]. As can be seen from Fig. 5b and Fig. 5e, the increase of cross-section moment between 30 – 50° is fastest for the

St900_1 grade, which has the lowest strain-hardening. This indicates that the contact point shift and multi-breakage happen faster for materials with lower strain-hardening. This conclusion is also supported by the fact that the decrease of the Z-displacement after 40° is also fastest for the St900_1 grade, meaning that the punch-sheet separation is largest, due to the pronounced multi-breakage effect.

Fig. 6 presents the peak strain, cross-section moment, Z-displacement and their first derivatives measured from 500 MPa and 700 MPa steels bent using punch radii R_p = 0.66 t, R_p = 2 t, and R_p = 4 t. As can be seen from Fig. 6a and Fig. 6d, the development of the peak strain and strain rate for the presented tests start out roughly identical, as most of the deformation is still elastic, but diverge after around 10°– 20° bend angle when the work-hardening properties come into effect. The peak strain increases at a higher rate for the St700 grade in all tool setups. For the St700 grade bent with the largest punch (R_p = 4 t) the strain rate starts to gradually decrease after 30° bend angle, and a steady state is reached at around 50°. For the St500 grade bent with the largest punch, the decrease of the strain rate starts already at around 15°, but the steady state is still reached at around 50°. For both materials bent with the medium punch (R_p = 2 t), the strain rate starts to gradually decrease after 40°, reaching a steady state around after 80°. With the smallest punch (R_p = 0.66 t), the difference between the materials is noticeable. For the St700 grade, the strain rate keeps increasing until around 85°. Whereas for the St500 grade, the strain rate decreases between 15 – 20°, then remains roughly constant before starting to decrease again after around 75°.

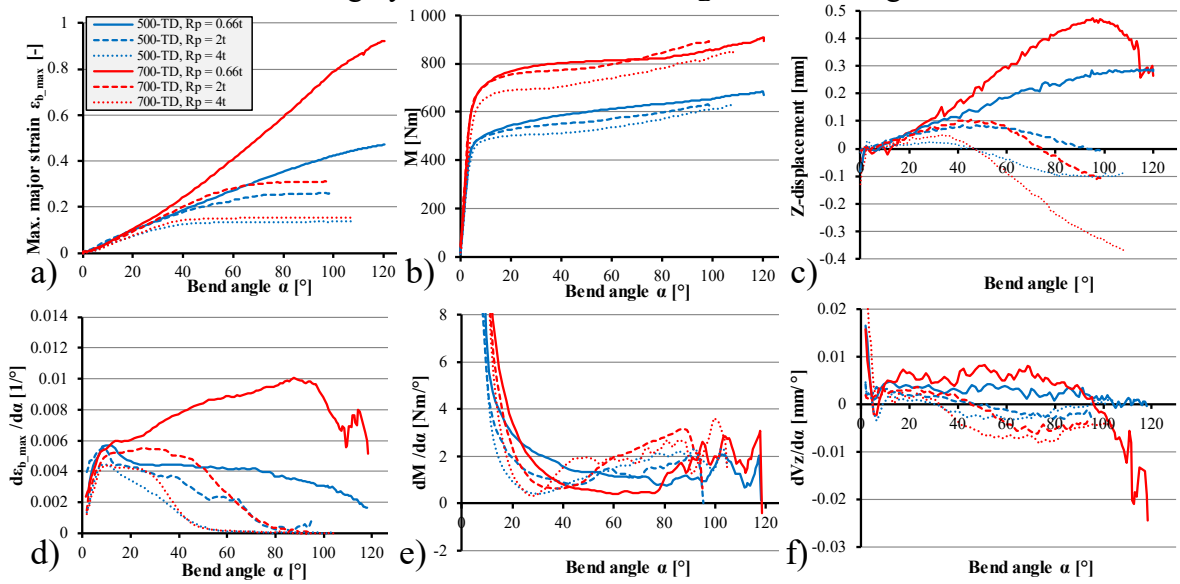

Fig. 6. Development of a) the peak strain, b) cross-section moment, c) Z-displacement, d) peak strain derivative, e) moment derivative and f) Z-displacement derivative, from St500 and St700 grades bent in transverse (TD) orientation with punch radii R_p = 0.66 t, R_p = 2 t and R_p = 4 t.

From Fig. 6e it is seen that for both materials, the moment derivative dM/dα reaches a minimum and starts to increase again at around 30°, 40° and 80° for the largest punch (R_p = 4 t), medium punch (R_p = 2 t) and smallest punch (R_p = 0.66 t), respectively. For the St700 grade, these angles correspond to the angles at which the strain rate first starts to decrease. For the St500 grade, the connection between the strain rate curve and the moment derivative curve is not as clear, due to the changes in the strain rate being more gradual and due to the initial decrease in strain rate after 15°. However, it is still assumed that the wrap-around angle coincides with the dM/dα minimum for both materials. It can also be seen here that for all three tool setups, the St700 grade has a lower dM/dα value at the wrap-around angle compared to the St500 grade, which again demonstrates that materials with lower strain-hardening, that produce more localized strain distribution, will also produce a lower dM/dα minimum.

Fig. 6c and Fig. 6f show the development of the Z-displacement and its derivative for the two grades and three setups. It is observed that the Z-displacement increases at a constant rate at the beginning for all tests but starts to decrease after a certain point. The start of the decrease of the Z-displacement derivative seems to coincide with the wrap-around angle determined from the moment derivative curves. The exception for this is the St500 grade with the smallest punch (R_p = 0.66 t), for which the changes in the Z-displacement are too gradual to discern from the measurement noise.

As discussed earlier, the start of the increase of the moment derivative dM/dα, as well as the decreases in the Z-displacement and strain rate, can be attributed to the wrap-around and multi-breakage effects, where the loading scheme changes, and the contact points shift away from the centerline. The wrap-around angle seems to decrease when punch radius is increased, which seems logical, as the wrap-around happens when the inside radius becomes equal to the punch radius.

Fig. 7 shows the correlation between the moment derivative dM/dα minimum value and two global formability measures: the uniform elongation A_{gt} from tensile tests and the peak bending strain ε_{b_max*} at 70° bend angle with punch radius R_p = 2 t. The strong correlation indicates that the moment derivative minimum is connected to the global formability properties of a material and that it may be possible to predict the peak bending strain from the moment derivative minimum.

The peak bending strain at a given angle has been deemed a decent measure for quantifying the strain distribution [17]. The connection between the peak strain and the cross-section moment implies that it may be possible to predict the development of the strain distribution using only the force-displacement data of a press brake, circumventing the need for strain measurement. This would also mean that the effects of the strain distribution, such as the shape of the bent sheet, inner radius, thinning, bend allowance, multi-breakage and punch-sheet separation could be predicted from the measured cross-section moment.

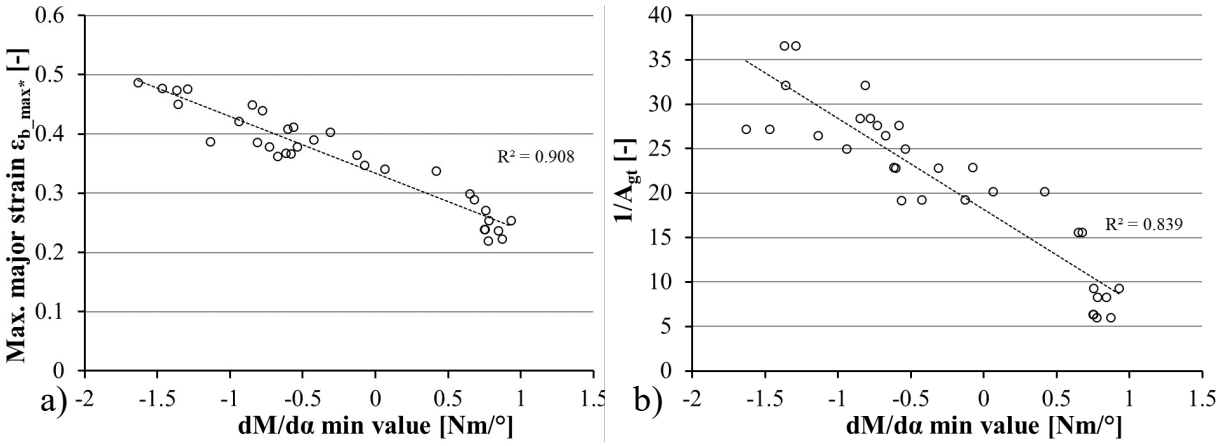

*Fig. 7. Moment derivative dM/dα minimum value as a measure of global formability. a) Correlation with the peak strain ε_{b_max*} measured at α = 70° from specimens bent using punch radius R_p = 2t; b) Correlation with the uniform elongation measured from tensile tests. *corrected for thickness variation [1].*

In other words, by measuring punch travel and force with sufficient accuracy during the first 30 – 40°, it may be possible to predict the behavior and shape of the bent workpiece during the rest of the bending process. This information could be used for adjusting the process parameters on the fly (so-called "adaptive control"), which could potentially lead to increased accuracy in the dimensions of the final product, fewer failed parts, as well as decreasing the time and resources spent on determining the correct process parameters through test bends.

Summary

In this paper, the formability of nine hot rolled steel grades with various strengths and ductility properties were investigated by air-bending tests using three different setups. The developments of the strain distribution, Z-displacement, and cross-section moment were measured throughout the bending process. The aim of the paper was to investigate the connection between the cross-section moment and other phenomena related to air-bending, such as the strain distribution development and the multi-breakage effect. The main observations and conclusions are summarized as follows:

- The wrap-around and multi-breakage can be detected from the derivative curves of the peak strain, cross-section moment and Z-displacement.
- Materials with lower strain-hardening are found to have lower minimum value of the cross-section moment derivative $dM/d\alpha$ at the wrap-around angle, as well as higher peak strain on the outer surface.
- The wrap-around angle is smaller for materials with low strain hardening, as well as when a larger punch radius is used.
- A connection between the peak strain and the cross-section moment implies that it may be possible to estimate the strain distribution in bending from the force-displacement curve of the punch.

Acknowledgments

Financial assistance of the Business Finland, project FOSSA– Fossil-Free Steel Applications, is acknowledged.

References

[1] A.-P. Pokka, V. Kesti, A. Kaijalainen, Global formability and bendability of ultra-high strength steels: Effect of mechanical properties on the strain distribution and behaviour in air-bending, Mater. Today Commun. 37 (2023), 107081. https://doi.org/10.1016/j.mtcomm.2023.107081

[2] A.-P. Pokka, A.-M. Arola, A. Kaijalainen, V. Kesti, J. Larkiola, Strain distribution during air bending of ultra-high strength steels, ESAFORM 2021 (2021). https://doi.org/10.25518/esaform21.2509

[3] S. D. Benson, Press Brake Technology: A Guide to precision sheet metal bending, Society of Manufacturing Engineers, Dearborn, Michigan, 1997.

[4] V. Vorkov, R. Aerens, D. Vandepitte, J. R. Duflou, The Multi-Breakage Phenomenon in Air Bending Process, Key Eng. Mater. 611–612 (2014) 1047–1053. https://doi.org/10.4028/www.scientific.net/KEM.611-612.1047

[5] A. Väisänen, K. Mäntyjärvi, J. A. Karjalainen, Bendability of Ultra-High-Strength Steel, Key Eng. Mater. 410–411 (2009) 611–620. https://doi.org/10.4028/www.scientific.net/KEM.410-411.611

[6] J. Heikkala, A. Väisänen, Usability Testing of Ultra High-Strength Steels, Proc. ASME 2012 11th Biennial Conference on Engineering Systems Design and Analysis 4 (2012) 163–173. https://doi.org/10.1115/ESDA2012-82770

[7] V. Kesti, A. Kaijalainen, A. Väisänen, A. Järvenpää, A. Määttä, A.-M. Arola, K. Mäntyjärvi, R. Ruoppa, Bendability and Microstructure of direct quenched Optim® 960QC, Mater. Sci. Forum 783-786 (2014) 818–824. https://doi.org/10.4028/www.scientific.net/MSF.783-786.818

[8] A.-M. Arola, V. Kesti, R. Ruoppa, The effect of punch radius on the deformation of ultra-high strength steel in bending, Key Eng. Mater. 639 (2015) 139–146.

[9] L. Wagner, H. Schauer, H. Pauli, J. Hinterdorfer, Improved bendability characterization of UHSS sheets, IOP Conf. Ser. Mater. Sci. Eng. 651 (2019) 012019. https://doi.org/10.1088/1757-899X/651/1/012019

[10] K. Cheong, J. Noder, A. Zhumagulov, C. Butcher, Characterization and Prediction of Plane Strain Bendability in Advanced High-Strength Steels, Metals 13 (2023) 1711. https://doi.org/10.3390/met13101711

[11] M. Kaupper, M. Merklein, Bendability of advanced high strength steels - A new evaluation procedure, CIRP Ann. - Manuf. Technol. 62 (2013) 247–250. https://doi.org/10.1016/j.cirp.2013.03.049

[12] K. Cheong, K. Omer, C. Butcher, R. George, J. Dykeman, Evaluation of the VDA 238-100 Tight Radius Bending Test using Digital Image Correlation Strain Measurement, J. Phys. Conf. Ser. 896 (2017) 12075. https://doi.org/10.1088/1742-6596/896/1/012075

[13] A.-M. Arola, A. Kaijalainen, V. Kesti, A.-P. Pokka, J. Larkiola, Digital image correlation and optical strain measuring in bendability assessment of ultra-high strength structural steels, Procedia Manuf. 29 (2019) 398–405. https://doi.org/10.1016/j.promfg.2019.02.154

[14] S. Gothivarekar, S. Coppieters, A. Van de Velde, D. Debruyne, Advanced FE model validation of cold-forming process using DIC: Air bending of high strength steel, Int. J. Mater. Form. 13 (2020) 409–421. https://doi.org/10.1007/s12289-020-01536-1

[15] R. Ruoppa, R. Toppila, V. Kesti, A. Arola, Bendability tests for ultra-high-strength steels with optical strain analysis and prediction of bending force, Proc. METNET Seminar 2014 Moscow (2014) 68–78.

[16] C. Suppan, T. Hebesberger, A. Pichler, J. Rehrl, O. Kolednik, On the microstructure control of the bendability of advanced high strength steels, Mater. Sci. Eng. A 735 (2018) 89–98. https://doi.org/10.1016/j.msea.2018.07.080

[17] A.-P. Pokka, V. Kesti, A. Kaijalainen, Total strain on the outer surface of steel sheets in air bending, Mater. Res. Proc. 28, (2023) 695–704. https://doi.org/10.21741/9781644902479-75

[18] L. Troive, New method for evaluation of bendability based on three-point-bending and the evolution of the cross-section moment, J. Phys. Conf. Ser. 896 (2017) 12006. https://doi.org/10.1088/1742-6596/896/1/012006

[19] C. Wang, G. Kinzel, T. Altan, Mathematical modeling of plane-strain bending of sheet and plate, J. Mater. Process. Technol. 39 (1993) 279–304. https://doi.org/10.1016/0924-0136(93)90164-2

[20] SFS-EN ISO 7438:2016: Metallic materials – Bend test.